NASA
Technical
Paper
2210

September 1983

Experiments in a Three-Dimensional Adaptive-Wall Wind Tunnel

Edward T. Schairer

NASA

25
25th Anniversary
1958-1983

NASA
Technical
Paper
2210

1983

Experiments in a Three-Dimensional Adaptive-Wall Wind Tunnel

Edward T. Schairer
Ames Research Center
Moffett Field, California

NASA
National Aeronautics
and Space Administration

**Scientific and Technical
Information Branch**

NOMENCLATURE

b model span (wing semispan), cm

C_L lift coefficient

$\bar{c}$ model mean aerodynamic chord, cm

H test section half-height, cm

L test section width, cm

M Mach number

p static pressure

p_T total pressure

U free-stream velocity, m/sec

u local streamwise velocity, m/sec

w vertical velocity, m/sec

x axial distance from quarter-chord (positive downstream), cm

y distance outboard of wing root, cm

z distance above wing, cm

α angle of attack, deg

ϕ perturbation velocity potential

Γ circulation, m^2/sec

Subscripts

a antisymmetric

s symmetric

SUMMARY

Three-dimensional adaptive-wall experiments were performed in the Ames Research Center (ARC) 25- by 13-cm indraft wind tunnel. A semispan wing model was mounted to one sidewall of a test section with solid sidewalls, and slotted top and bottom walls. The test section had separate top and bottom plenums which were divided into streamwise and cross-stream compartments. An iterative procedure was demonstrated for measuring wall interference and for adjusting the plenum compartment pressures to eliminate such interference. The experiments were conducted at a freestream Mach number of 0.60 and model angles of attack between 0 and 6°. Although in all the experiments wall interference was reduced after the plenum pressures were adjusted, interference could not be completely eliminated.

I. INTRODUCTION

The flight conditions of modern aircraft are difficult to simulate in conventional solid- and porous-wall wind tunnels without significant wall interference. When configurations are tested at high lift or at transonic speeds, analytical or empirical corrections for wall interference are uncertain because the governing equations are nonlinear, and the conditions at the tunnel walls are often unknown. Although wall interference can be minimized by restricting the size of the model tested in a particular wind tunnel, this approach reduces the useful Reynolds number capability of that wind tunnel and makes inefficient use of the test section space and airstream energy.

Wall interference can be eliminated by adjusting conditions at the tunnel walls. If a streamtube containing the model is shaped as though the model were in free air, then flow within the streamtube (e.g., at the model) would be the same as free-air flow regardless of the proximity of the tunnel walls.

Two-dimensional wind tunnels with adjustable walls were successfully demonstrated in England during World War II (ref. 1-3). These tunnels were developed to avoid choking at high speeds. Solid, flexible walls were bent to conform to free-air streamlines whose shapes were determined by calculating flow past the model in free air. This approach was practical only for flows that were simple enough to be represented mathematically. After the war, ventilated walls were accepted as the best solution to the choking problem, and flexible-wall tunnel research was discontinued.

In 1973, Ferri and Baronti (ref. 4) and Sears (ref. 5) simplified the task of determining free-air wall conditions. They independently showed that free-air conditions can be estimated on a surface surrounding a model from measurements of actual conditions on the same surface. No knowledge about the model or the flow inside the surface is required. Sears showed that wall conditions can be adjusted until the measured and estimated free-air conditions on the control surface are the same. This method is the basis of the "adaptive-wall" wind tunnel.

Large reductions in two-dimensional, transonic wall interference have been achieved in small adaptive-wall wind tunnels in Europe and the United States. In two dimensions, the number of measurements required to assess interference is manageable, and only the top and bottom walls need to be adjustable. Fast and automatic procedures for eliminating interference have been demonstrated. Wall adjustments have been made either by deforming flexible, solid walls (refs. 6-13) or by controlling the flow of air through rigid, ventilated walls (refs. 14-21). Test sections of both types have been, or are being, built for production wind tunnels (ref. 22).

Adaptive-wall experiments in three-dimensional tunnels have been less conclusive than those in two-dimensional tunnels. Wall interference is usually less severe in three dimensions than in two, and thus is more difficult to measure. Furthermore, interference must be measured and controlled on a surface surrounding the model, rather than just along lines above and below the model.

The flexible-wall approach to adaptive walls is awkward in three dimensions because the wall shapes required to eliminate interference include double curvature. This problem has been dealt with in a variety of ways. At the University of Southampton, a two-dimensional 6- by 6-in. test section with flexible top and bottom walls was used to eliminate choking of flow past a three-dimensional model. However, substantial differences with free-air data remained (ref. 12). Better approximations of free-air, three-dimensional flows have been obtained at the Technical University of Berlin in

an 18- by 15-cm octagonal test section in which each wall can be bent in two dimensions (ref. 13). At the Deutsche Forschungs-und Versuchsanstalt für Luft-und Raumfahrt (DFVLR), a deformable, cylindrical, rubber test section has been built (ref. 13). Finally, at the Air Force Flight Dynamics Laboratory (AFFDL), a test section with top and bottom walls composed of flexible rods has been demonstrated (ref. 23).

Problems with double curvature are avoided in adaptive-wall test sections with rigid, ventilated walls. Airflow through the walls is controlled either by adjusting the porosities of separate wall panels or by locally controlling the pressure difference through the wall by means of a compartmentalized plenum. Wall panels or plenum compartments can be arranged to permit simultaneous adjustment of streamwise and cross-stream wall conditions.

Three-dimensional adaptive-wall experiments were conducted at Arnold Engineering Development Center (AEDC) in the 4T Tunnel (ref. 24). The porosity of each perforated wall was independently adjusted to minimize wall interference. The experiments showed that more independently controllable wall panels were needed to eliminate interference. A new test section with 64 panels has been built and will be demonstrated in the AEDC 1T Tunnel (ref. 25).

At ARC, adaptive-wall test sections with slotted walls and compartmentalized plenums have been developed. The ventilated-wall approach was selected because of its advantages in three-dimensional applications. Slotted, rather than porous, walls were selected because of the wide use of slotted-wall test sections at Ames, and because windows can be placed between slots, thus permitting the use of optical flow measurement techniques.

Two-dimensional airfoil experiments in the Ames 25- by 13-cm adaptive-wall test section were completed in 1980 (ref. 21). These experiments were successful up to airspeeds at which supersonic flow penetrated the interference assessment surfaces. The success of the experiments was limited at higher speeds because linear theory was used to assess interference, and because at high speeds the flow in the tunnel became unsteady. The experiments demonstrated a new, two-surface interference assessment procedure; the use of laser velocimetry for making flow measurements; influence coefficients for determining wall adjustments; and automatic, on-line control by a minicomputer.

This paper describes a three-dimensional adaptive-wall experiment which was also performed in the 25- by 13-cm test section. The purpose of the experiment was to determine how successfully the procedures used in the two-dimensional experiment could be extended and applied to a three-dimensional configuration. In the two-dimensional experiment, conditions at the upper and lower walls could be adjusted in the streamwise direction. For the three-dimensional experiment, the test section was modified so that conditions at the slotted upper and lower walls could also be varied in the cross-stream direction. The sidewalls were solid. The model was a semispan wing which was mounted to one sidewall (fig. 1). The laser velocimeter was modified to allow measurements to be made at different cross-stream locations, and a three-dimensional interference assessment algorithm was developed.

II. ADAPTIVE-WALL PROCEDURE

The adaptive-wall procedure used in the ARC two- and three-dimensional experiments was developed by Davis (ref. 26) and is a modification of Sears' approach. Whereas Sears' method requires that two flow quantities be measured on one surface surrounding the model, Davis' method requires that only one flow quantity be measured but on two surfaces.

In the ARC experiments, the distribution of vertical velocity (upwash) was measured on two imaginary surfaces surrounding the model (fig. 2). The measurements were made with a laser velocimeter. The upwash distribution on the surface closest to the model (source surface) was used as one boundary condition in a mathematical representation of the flow in the region beyond the source surface (outer flow); the free-air upwash distribution was imposed on a second, fictitious far-field boundary beyond the wind tunnel walls. The resulting boundary value problem was solved for the free-air upwash distribution at the outer surface (field surface).

Wall interference was measured by comparing the measured and computed upwash distributions at the field surface. Differences between the distributions were used as a basis for making wall adjustments. Wall conditions were adjusted by changing the pressures in the compartments of a segmented plenum. The required pressure changes were computed using empirical influence coefficients. Wall adjustments produced velocity changes at the model and the source surface, as well as at the field surface. Thus, the adaptive-wall procedure was repeated until the measured and free-air upwash distributions at the field surface were compatible.

III. APPARATUS

A. Test Section

The experiment was conducted in the Ames 25- by 13-cm atmospheric indraft wind tunnel. The test section used in the two-dimensional experiments was modified for the three-dimensional experiments to permit cross-stream control of conditions at the upper and lower walls (fig. 3). Except for this change, the basic features of the test section were retained. The upper and lower walls were slotted and had an

open area ratio of 0.12 and a divergence angle of 0.10°. The sidewalls were solid plexiglass.

As in the two-dimensional experiments, separate plenums above and below the test section were divided into streamwise compartments. The number of streamwise compartments was reduced from 10 for the two-dimensional experiments to 7 for the three-dimensional experiments. Compartments nearest the model, where streamwise upwash gradients were expected to be largest, were smaller than compartments upstream and downstream of the model. For the three-dimensional experiments, each compartment was subdivided into three cross-stream compartments of approximately equal size.

The auxiliary air system used to adjust the wall conditions in the two-dimensional experiments was expanded from 20 to 36 channels for the three-dimensional experiments. Eighteen upper and 18 lower plenum compartments were connected to a vacuum manifold and to ambient room air (fig. 4). An ejector, which could operate continuously for about 30 min, maintained the pressure in the manifold at 35.5 cm (14 in.) Hg (absolute).

The rigid sidewalls could not be adjusted. For a wing-on-a-wall configuration this was not expected to be particularly restrictive. The sidewall on which the wing was mounted was assumed to be a plane of symmetry and thus required no adjustments. Interference due to the opposite sidewall was expected to be much less than that due to the top and bottom walls, because the model span was greater than the tunnel height.

B. Model

The model (fig. 5) was a scaled-up (1.6 times) replica of a semispan wing tested at Langley Research Center in 1951 (ref. 27). It was selected for the experiment because of the essentially free-air data which were available from the Langley tests. Forces and moments on the model were measured by a six-component force and moment balance. The blockage ratio of the model in the adaptive-wall test section was 0.026, and the span to tunnel height ratio was 1.31. As in the Langley test, all the experiments were performed without a boundary-layer trip.

C. Balance

The model was supported at its quarter-chord by a 0.75-in. TASK XXIXB internal strain gauge balance. To accommodate the collecting optics of the laser velocimeter, the balance support (fig. 5) was designed to block as little as possible of the view through the transparent sidewall. The balance protruded through a hole in the sidewall with its longitudinal (roll) axis oriented perpendicular to the sidewall. A shroud, attached to the outside of the sidewall, enclosed the balance and supported it at its tapered end. Angle of attack was measured with a gunner's quadrant (bubble-type inclinometer) and was changed by rotating the balance and model assembly within the support shroud. A 0.45-mm gap between the model root and the tunnel sidewall provided clearance between the model and the sidewall when the balance deflected under loads.

The output from each of the six strain gauges in the balance was amplified and input into one channel of the minicomputer analog-to-digital (A-to-D) converter. The raw data were reduced on-line by the minicomputer. The balance was check-loaded by applying known loads at the aerodynamic center of the model. Normal force data were accurate to within 2% of the applied loads.

D. Laser Velocimeter

Laser velocimetry (LV) was used to measure upwash distributions at the source and field surfaces. LV is a nonintrusive and accurate technique that had been used successfully in the two-dimensional experiments. The principal disadvantage in using LV was that acquiring data at many widely separated points was time-consuming. This problem was particularly severe in the three-dimensional experiment since measurements were required at many points to define the velocity fields at the source and field surfaces.

The laser velocimeter used in the two-dimensional experiments was modified so that measurements could be made at different spanwise locations (fig. 6). A third, cross-stream, stage was added to the positioning platforms which carried the transmitting and collecting lenses. Each stage was moved by a lead screw driven by a stepping motor. The motors were automatically operated by a six-channel, programmable controller which was commanded by the minicomputer.

Signal processing was identical to that used in the two-dimensional experiment. The flow was not seeded, and data rates of 500 to 1000 bursts/sec were typical. Each mean velocity measurement was based on 1000 bursts.

During calibration of the test section, the laser velocimeter was used to measure streamwise and vertical velocity profiles. Switching between the two velocity components was accomplished by rotating a dove prism in the path of laser beams.

During the adaptive-wall experiments, LV measurements were made at 98 points on the source and field surfaces. The number of these "control" points was limited by the time allowed for making the measurements (about 20 min). The points were distributed (fig. 3) to provide representations of the upwash distributions as accurately as possible. On the upper and lower faces of the field surface, one control point was centered below and above each plenum compartment, respectively. This arrangement yielded a particularly simple influence coefficient matrix (see Section VI). The coordinates

of the control points, normalized with respect to the model mean aerodynamic chord and span, are given in figure 7.

Consecutive sets of LV upwash measurements at the control points could be repeated with a root-mean-square (rms) difference between sets of about 0.30 m/sec. At Mach 0.60, this is a flow-angle uncertainty of ±0.086°. Sets of data agreed within ±0.50 m/sec at 90% of the measurement points, and differences larger than 0.70 m/sec almost never occurred. Repeated mean upwash measurements at a fixed point typically had an rms variation of about 0.15 m/sec and a maximum difference between readings of 0.60 m/sec.

E. Pressure Instrumentation

Static pressures were measured at 2.54-cm intervals along the centerline of the inboard sidewall and in each of the 36 plenum compartments (fig. 3). Static pressure in the bell mouth of the tunnel inlet (upstream of the contractions and downstream of the settling screens) was assumed to be equal to the total pressure in the test section.[1] The total temperature was measured by a thermocouple in the tunnel inlet.

Each pressure orifice was connected to one of four Scanivalve pressure transducers. The Scanivalves were automatically stepped and homed by a controller activated by the minicomputer. The outputs of each Scanivalve and of the thermocouple were amplified and connected to the minicomputer A-to-D converter. The data were automatically reduced to physical units and were graphically displayed on a CRT after each set of pressure measurements was acquired.

F. Computer

The experiment was automatically controlled by a Data General Eclipse minicomputer. Tasks performed by the computer included data acquisition and reduction, and calculations of free-air conditions and plenum compartment pressure changes. The only tasks not controlled by the minicomputer were the plenum compartment valve adjustments, which were made manually according to the computer's calculations.

Thirteen channels of analog data and one channel of digital data were read by the minicomputer during each cycle of the adaptive-wall procedure. Each analog channel was sampled 200 times at 1-msec intervals, and the mean value was taken as the channel output. The digital channel was LV data, and each data point was based on 1000 readings (ref. 21).

[1] During calibration of the empty test section, a Pitot tube was used to measure total pressure. LV measurements downstream of the tube revealed a substantial wake which would have impinged upon the model. Thus, after the model was installed, the Pitot tube was not used.

The minicomputer automatically switched each instrument to its proper position or configuration by means of relay closures. Thus, the computer activated the step and home switches to the Scanivalve controller, switched the calibration shunt resistors in and out of the balance bridges (tunnel off), and commanded the LV positioner to move to its next step.

Data reduction was performed on-line, and the reduced data were displayed in tables and graphs at a graphic display terminal. Hard copies of the display could be made with an electrostatic copier.

IV. OUTER FLOW CALCULATION

The flow in the region beyond the source surface was assumed to be governed by the three-dimensional, linearized, compressible-flow equations. These equations were solved by an approximate, finite-difference scheme similar to a solution developed by Davis (ref. 26).

The outer region, which in principle extended outward from the source surface to infinity, was approximated by a finite space truncated by far-field boundaries (fig. 8). The plane of the inboard sidewall was assumed to be a plane of symmetry. The free-air upwash distribution at the far-field boundaries was assumed to be equal to that produced by a horseshoe vortex at the position of the model.

The upper and lower faces of the source surface were located just above and below the obstruction produced by the balance support. The vertical face of the source surface was located outboard of the tip of the model at approximately the position of maximum upwash.

The field surface was located between the source surface and the test section walls. The upper and lower faces were chosen to be as close to the walls as possible without being in the wall boundary layer or in the regions where local disturbances due to individual slots were dominant.

The mesh used in the outer-flow calculation was stretched in all three directions and was designed to be consistent with the LV measurement points (fig. 9). In the streamwise direction, the mesh at the source surface coincided exactly with the LV measurement points, and no interpolation was required. In the cross-stream direction, however, there were more computation points (9) at the source surface than LV measurement points (3). Boundary conditions at the intermediate points were determined by linear interpolation between the LV data. On the vertical face of the source surface, conditions at intermediate grid points were determined by a second-order interpolation.

Davis posed the outer-flow problem directly in terms of vertical velocity (w) by differentiating the potential equation with respect to the vertical coordinate (z), reversing the order of differentiation, and replacing $\partial\phi/\partial z$ with w. Thus

$$\frac{\partial^2 \phi}{\partial x^2} + \frac{\partial^2 \phi}{\partial y^2} + \frac{\partial^2 \phi}{\partial z^2} = 0$$

became

$$\frac{\partial^2 w}{\partial x^2} + \frac{\partial^2 w}{\partial y^2} + \frac{\partial^2 w}{\partial z^2} = 0 \qquad (1)$$

This form was convenient because it allowed the measured vertical velocity distribution at the source surface to be used directly as a Dirichlet boundary condition.

The central difference approximation to equation (1) was solved directly along each vertical line, and by iteration in the cross-stream and streamwise directions. The computation was continued until the solution ceased to change with each successive iteration. This occurred after 20 iterations and required about 30 sec of computation time on the minicomputer. The computer speed was approximately 0.50 million floating-point operations/sec.

As a check case, the outer-flow solution was computed for a horseshoe vortex in free air. Vertical velocities induced by the vortex were imposed as boundary conditions at the control points on the source surface and at the far-field boundary. Boundary conditions at the intermediate mesh points on the source surface were interpolated as described above. Figure 10 compares the resulting outer-flow solution at the field surface with the horseshoe vortex solution. The agreement at the inboard rows of control points (figs. 10(a),(b)) is very good, but the agreement becomes progressively worse at the more outboard locations.

The errors at the upper face of the field surface (figs. 10(a),(c),(e)) were due to interpolation of boundary conditions at the source surface. This was verified by repeating the outer-flow calculation with boundary conditions at *all* the mesh points on the source surface defined by the horseshoe vortex (no interpolation between control points). The agreement between the recomputed outer flow and the horseshoe vortex solutions was excellent except at the points outboard and in the plane of the vortex (fig. 10(g)). The residual errors at these in-plane points occurred because the computational mesh was too coarse to resolve the enormous spanwise upwash gradient near the trailing vortex. Since wall interference at the outboard, in-plane points (fig. 10(g)) was not used to compute wall adjustments (see Section VI), errors in the outer-flow solution at these points were of little consequence in the adaptive-wall experiments.

V. EMPTY TUNNEL CALIBRATION

The original test plan called for adaptive-wall experiments at $M = 0.60$ and 0.70. To save time, the empty test section was calibrated and influence coefficients were measured only at $M = 0.70$. Passive-wall experiments were performed with the model installed at both $M = 0.60$ and 0.70; however, time constraints permitted adaptive-wall experiments at $M = 0.60$ only.

The empty test section was calibrated with the upper and lower wall slots open and without sucking or blowing. The axial Mach number distribution was determined from total pressure and sidewall static pressure measurements. Surveys of the axial and vertical velocity fields were also made with the laser velocimeter.

The sidewall pressure data indicated that between $x = -1.5\ \bar{c}$ and $x = 3.0\ \bar{c}$ the Mach number was nearly constant. The standard deviation of the axial Mach number distribution in this region was typically 0.002.

Measurements with the laser velocimeter revealed a pair of longitudinal vortices extending the length of the test section near each sidewall. These vortices were characterized by adjacent regions of upwash and downwash, higher than freestream turbulence intensity, and lower than freestream axial velocity. They were apparently produced at each corner of the two-dimensional contraction upstream of the test section. Evidence of the vortices is presented in figures 11 and 12.

No attempt was made to eliminate the corner vortices. Their effects on the experiments with the model installed are discussed in Section IX, D.

VI. INFLUENCE COEFFICIENTS

An empirical constant or "influence coefficient" was used to describe the change in vertical velocity produced at a point at the field surface by a change in pressure in one plenum compartment. Each control point was related to every compartment by such a constant. The resulting set of linear equations was solved to find the compartment pressure changes which would produce the desired velocity changes at all the control points.

Each control point at the upper and lower faces of the field surface was positioned immediately below and above one plenum compartment, respectively.[2] This arrangement produced a square, diagonally dominant, influence-coefficient matrix in which most of the off-diagonal terms were zero. The cross-stream influence of a compartment decayed rapidly beyond the physical extent of the compartment, and was essentially zero at cross-stream control points (fig. 13). Furthermore, control points at the upper face of the field surface were not affected by pressure changes in lower compartments, and vice versa. Only in the streamwise direction was the influence of a compartment felt at more than one control point (fig. 14). Thus, control of each axial

[2] Although LV measurements were made at a seventh control point on each axial line, data at these points were not used in the wall adjustment calculation.

row of control points was uncoupled from control of the other rows. Control points outboard and in the plane of the wing were not used to compute plenum pressure changes because the influence coefficients at these points were zero.

Influence coefficients were measured at $M = 0.70$ in the empty test section by changing the pressures in the plenum compartments, one at a time, and measuring the upwash at the control points with the laser velocimeter. Each influence coefficient was determined from the slope $\Delta w/\Delta p$ for small pressure changes (fig. 15). The influence coefficient was different depending upon whether air was being injected into or removed from the compartment.

VII. PASSIVE-WALL EXPERIMENTS

The model was tested in two "passive-wall" configurations: one with the wall slots open, but without suction or blowing, and the other with the slots taped, simulating solid walls. The "passive slotted wall" configuration differed from passive walls in a conventional ventilated test section since the plenum partitions prevented circulation of the air in the upper and lower plenums. In addition, in the passive slotted-wall configuration there was no net mass flow into or out of the test section through the walls.

For both passive-wall configurations, forces on the model and vertical velocities at the source and field surfaces were measured as functions of angle of attack and Mach number. Upwash measurements at the adaptive-wall control points were used to compute the passive-wall interference.

The uncorrected lift-curve (C_L versus α) of the model is compared with the reference free-air data in figure 16. The effect of the tunnel walls was to increase the lift relative to the free-air data. For the same angle of attack, the model lift with the walls taped was slightly higher than the lift with passive slotted walls. These effects were expected and are discussed in Section IX,C.

Figure 17 illustrates upwash distributions measured along axial lines on the source surface above and below the model ($M = 0.70$, $\alpha = 5.3^\circ$, passive slotted walls). The detailed profiles (solid lines) are compared with the profiles obtained by linear interpolation between the data at the adaptive-wall control points (dashed lines). Below the wing, measurements at the control points are representative of the actual profile. Above the wing, where the vertical velocity gradients are greater, the comparison is not as good.

Figure 18 is a similar comparison of the upwash distributions measured along two spanwise lines downstream of the wing. Linear interpolations between the three spanwise control points crudely approximated the actual profile. The effects of these interpolation errors on the accuracy of the outer flow solution were discussed (for the case of a horseshoe vortex) in Section IV.

The upwash measured at the field surface control points is compared with the free-air upwash predicted in the outer-flow calculation for the case $M = 0.60$, $\alpha = 5.3^\circ$, and taped slots in figure 19. The interference was greatest downstream of the model quarter chord. Inboard and downstream of the wing tip, the computed downwash was greater than the measured downwash. Outboard of the wing tip, the computed upwash was greater than the measured upwash. This trend recurred in all subsequent experiments.

The rms difference between the measured and computed velocities at the field surface control points was used as a quantitative measure of wall interference. This difference was 1.56 m/sec for the solid-wall case illustrated in figure 19.

VIII. ADAPTIVE-WALL EXPERIMENTS

Adaptive-wall experiments were performed at $M = 0.60$ and $\alpha = 5.3^\circ$ and 2.0°. The experiments began with passive slotted walls and continued for three to five cycles of wall adjustments. In general, the experiments were terminated by equipment failures or loss of the use of the compressor which drove the tunnel. Because of these problems, the experiments were restarted several times.

The time available for each cycle of the adaptive-wall procedures was limited by the ejector, which could operate continuously for only about 30 min. At the end of each cycle, the wind tunnel was shut down so that the compressor could repressurize the storage sphere which drove the ejector.

Table 1 summarizes how the time available for each cycle was budgeted. Collection of the LV data consumed about half of the available time. The time available for valve adjustments was not long enough to allow the pressures in all 36 plenum compartments to be changed. Consequently, pressure changes were made only in those compartments that influenced the velocities at control points where wall interference was largest. This limited the degree to which wall interference could be reduced during each cycle.

Figure 20 compares the outer-flow solution with the upwash distribution measured at the field surface for the case $M = 0.60$, $\alpha = 5.3^\circ$, passive slotted walls. The rms difference was 1.38 m/sec. After two cycles of wall adjustments, the rms difference was reduced to 0.89 m/sec (fig. 21).

The outer-flow calculation consistently underestimated the velocity changes needed to eliminate wall interference. Because of this, a relaxation factor of 2.0 was used to compute wall adjustments.

Figure 22 illustrates how the pressures in the plenum compartments changed after two cycles of the adaptive-wall procedure ($M = 0.60$, $\alpha = 5.3^\circ$). Not all the pressure control valves were adjusted. Pressure changes in some compartments were induced solely by valve adjustments in neighboring compartments.

All the plenum compartments that were controlled by valve adjustments ("active control") were downstream of the model quarter chord. The intended effect of these adjustments was to increase the downwash downstream and inboard of the wing tip, and to increase the upwash downstream, outboard, and below the wing tip. Maximum available suction was applied to the two most-downstream, lower, inboard compartments. Figure 21(b) shows that additional suction would have been necessary in these compartments to eliminate wall interference.

Figures 23 and 24 summarize the initial and final interference assessments for the case $M = 0.60$, $\alpha = 2.0°$. The rms error was reduced from 1.08 to 0.74 m/sec. As in the $\alpha = 5.3°$ case, maximum suction was eventually applied to the two most-downstream, lower, inboard compartments. Figures 23 and 24 also include data from numerical simulations, which will be discussed in Section IX, B.

IX. DISCUSSION

It was evident from the on-line outer-flow calculations that wall interference was reduced by the adaptive-wall procedure, but was not completely eliminated. After the experiments were completed, the data were analyzed by other techniques. Specifically, interference was separated into contributions due to lift and blockage; the lift coefficient was compared with experimental free-air data; classical corrections for interference were applied to the lift data; and the lift and upwash data were compared with data from numerical simulations. Finally, sources of error in the adaptive-wall procedure were identified, and their effects on the outcome of the experiments were analyzed.

A. Lift and Blockage Interference

Lift- and blockage-induced wall interferences were measured independently by applying the outer-flow calculation to the symmetrical and antisymmetrical components of the upwash data, respectively. This separation was possible because the LV control points were arranged symmetrically above and below the plane of the wing. Thus

$$w_s(x,y,\pm z) = \frac{w(x,y,z) + w(x,y,-z)}{2} \qquad \text{(lift)}$$

$$w_a(x,y,\pm z) = \pm \frac{w(x,y,z) - w(x,y,-z)}{2} \qquad \text{(blockage)}$$

Lift interference was consistently greater than blockage interference. This is evident for the case $M = 0.60$, $\alpha = 5.3°$, and taped walls, illustrated in figure 25. The principal effect of lift interference was to decrease the magnitude of the downwash downstream and inboard of the wing tip. Outboard of the wing tip, the outer-flow solution was greater than the measured upwash. There was very little lift interference upstream of the wing quarter chord.

Figure 26 illustrates the effect of the adaptive-wall procedure on the lift interference for the case $M = 0.60$, $\alpha = 5.3°$, slotted walls. Large changes in lift-induced velocities were produced downstream of the wing quarter chord, and the lift interference was substantially reduced. The effects of wall adjustments on the blockage interference for the same case were relatively slight (fig. 27).

The effect of wall interference on the lift-induced upwash was interpreted by the classical method of images (ref. 28). According to this method, if the model is represented by a horseshoe vortex, then the boundary conditions at solid tunnel walls are satisfied by a doubly infinite array of image vortices (fig. 28). The wall-induced velocities are those due to the image vortices.

The outer-flow calculation was applied to the vertical velocity field induced by a horseshoe vortex in a solid-wall wind tunnel. Interpolation errors at the source surface were avoided, as discussed in Section IV. Figure 29 compares the outer flow solution at the field surface with the solution obtained by the method of images. The comparison is qualitatively the same as the lift-interference assessment of the model in the taped-wall test section (fig. 25).

Figure 29 also illustrates the vertical velocities induced by a horseshoe vortex in free air. At most of the control points, the outer flow solution lies between the solid-wall and free-air solutions. Outboard and downstream of the bound vortex, however, the directions of the velocity changes indicated by the free-air and outer-flow solutions conflict.

B. Comparison with Numerical Simulation

Upwash data at the field surface for the case $M = 0.60$, $\alpha = 2.0°$, were compared with a numerical, free-air solution (unpublished paper by Joel P. Mendoza, Ames Research Center) computed with a linear panel code (ref. 29). For the passive-wall condition (fig. 23), the outer-flow solution substantially underestimated the magnitudes of the vertical velocity changes needed to match the free-air data. For the most part, however, the directions of the velocity changes called for were correct. After five cycles of wall adjustments, the agreement between the experimental, numerical, and outer-flow data was much improved (fig. 24).

C. Lift Coefficient

The adaptive-wall procedure reduced the lift coefficient of the model at both angles of attack (fig. 30). At $\alpha = 5.3°$, the reduction was about half of that which was required to match the free-air data (ref. 27), thus indicating

undercorrection for wall interference. This is consistent with the undercorrection evident from the upwash data in figure 21.

At $\alpha = 2.0°$, the lift coefficient after the last cycle of wall adjustments was lower than the experimental free-air lift coefficient. The free-air coefficient computed by numerical simulation was higher than the experimental free-air lift coefficient (ref. 27). The reasons for these differences are not known.

Angle-of-attack corrections computed by the classical method of images were larger than were needed to reconcile the taped-wall lift data with the experimental free-air data (fig. 30). As formulated by Glauert (ref. 28), this method is accurate only when the span of the model (b) is small relative to the height of the wind tunnel ($2H$) – a condition clearly violated in the present experiment ($b/2/H = 1.31$). Corrections were computed by the method of images but *without* the assumption that $b/2/H \ll 1$. These corrections were smaller than were needed to match the free-air data.

Some of the differences between the adaptive-wall data and the free-air data (ref. 27) must be attributed to differences between the boundary layers on the inboard sidewalls in the two experiments. In reference 27, the model was mounted on a reflection plane located outside the tunnel boundary layer, and the effect of the wall boundary layer on the model was small. In the present experiment, the model was mounted to the inboard sidewall, and thus the root of the model was immersed in the wall boundary layer.

D. Errors

The greatest source of errors was in calculating the plenum compartment pressure adjustments necessary to produce the desired velocity changes. Although the effects of pressure changes in a single plenum compartment were predictable (fig. 15), linear superposition was not adequate to predict the combined effects of pressure changes in several compartments. Thus, required velocity changes could not be accurately produced. Although the first two or three cycles of wall adjustments were usually successful in reducing the overall interference, these reductions were never as large as expected. Wall adjustments beyond the third cycle usually did not further reduce the overall interference.

Desired velocity changes were produced with an accuracy of ±40%, or better, 50% of the time. Errors in excess of 100% occurred 14% of the time. In absolute terms, 50% of the velocity corrections were accurate to within ±0.50 m/sec, and 90% were accurate to within ±1.24 m/sec. There was no difference in accuracy between corrections applied by suction and blowing. Large and small velocity changes were produced with the same absolute uncertainty.

Interpolation of boundary conditions at the source surface introduced important errors in the outer-flow solution. Measurements were not made at enough points at the source surface to accurately represent the upwash distribution there. In particular, the spanwise variation in upwash was far too complex to be inferred from measurements at just three points at each streamwise location. Interpolation errors were largest outboard of the wing tip where the spanwise upwash gradient was large.

The accuracy of the experiments was not limited by the resolution or repeatibility of the LV data. The rms interference was always substantially larger than the rms repeatibility of the LV data sets.

The effect of the longitudinal vortices, measured during the tunnel calibration, on the adaptive-wall experiments is not known. Assuming their positions did not change significantly when the model was installed, the vortices lying along the inboard sidewall would have been confined within the source surface, and the vortices along the outboard sidewall would have been outside the field surface. As long as the flow at and between the source and field surfaces was inviscid and irrotational, the outer-flow calculation was not compromised. The inboard vortices can be considered as alterations of the model's shape and the outboard vortices as wall perturbations.

X. CONCLUDING REMARKS

This experiment showed that adaptive-wall procedures that had been demonstrated in two dimensions can be extended to reduce wall interference in a three-dimensional test section. Flow measurement, interference assessment, and wall control techniques were successfully combined into an efficient algorithm which was applied to a three-dimensional configuration. The success of the experiment was limited by the inability to accurately predict the effects of wall adjustments on the flow in the test section.

The experiment was the first demonstration of *local* wall control in a ventilated, three-dimensional test section. Previous attempts to reduce three-dimensional wall interference in a ventilated test section had been limited to *global* control of entire walls.

The following specific conclusions can be drawn:

1. Wall interference was successfully measured. The interference was large, and was not "correctable" by classical analytical methods. Vertical velocity, the quantity used in the interference assessment, was sensitive to lift-induced wall interference. Errors in measuring interference occurred because the boundary conditions at the source surface were not measured at enough points, especially in the cross-stream direction.

2. Wall interference was reduced after the pressures in the plenum compartments were adjusted. This was evident from (a) the on-line interference calculations, (b) comparisons of the measured upwash with upwash determined by numerical

simulation, and (c) comparisons of the measured lift coefficient with experimental free-air lift data.

3. The number of plenum compartments was sufficient to control the flow at the upper and lower faces of the field surface. The experiment did not establish whether adaptive sidewalls are needed to reduce wall interference to acceptable levels.

4. Measurable interference remained after several cycles of the adaptive-wall procedure. Efforts to eliminate the residual interference failed because (a) the linear influence coefficients did not accurately relate vertical velocity changes at the field surface to pressure changes in the plenum compartments, and (b) in several instances the available wall suction was insufficient to produce required velocity changes.

Based on this experiment, there is little doubt that three-dimensional wall interference can be eliminated in a research wind tunnel. Not all the techniques employed here, however, can be extrapolated to a large, production test section. The most formidable problem is that of measuring flow conditions at the interference assessment surfaces. Although conventional LV was feasible in the present experiment, it probably would not be practical in a large, production, three-dimensional test section. The time required to make the measurements would be prohibitively long. In addition, LV is very sensitive to small misalignments of optics and requires careful interpretation of the signal if reliable data are to be obtained.

It remains to be shown that three-dimensional free-air data can be extracted more easily from a test section with adaptive walls than from one with conventional passive walls. The present experiment did not resolve this question because the test section was not operated with conventional passive walls (i.e., without plenum partitions). Experiments are being planned which will compare the performance of a test section with adaptive and conventional passive walls.

Ames Research Center
National Aeronautics and Space Administration
Moffett Field, California 94035, May 9, 1983

REFERENCES

1. Preston, J. H.; and Sweeting, N. E.: The Experimental Determination of the Interference on a Large Chord Symmetrical Joukowski Aerofoil Spanning a Closed Tunnel. Aeronautical Research Committee, R&M No. 1997, Dec. 1942.

2. Preston, J. H.; Sweeting, N. E.; and Cox, D. K.: The Experimental Determination of the Two-Dimensional Interference on a Large Chord Piercy 12/40 Aerofoil in a Closed Tunnel Fitted with a Flexible Roof and Floor. Aeronautical Research Committee, R&M No. 2007, Sept. 1944.

3. Lock, C. N. H.; and Beavan, J. A.: Tunnel Interference at Compressibility Speeds Using the Flexible Walls of the Rectangular High-Speed Tunnel. Aeronautical Research Committee, R&M No. 2005, Sept. 1944.

4. Ferri, A.; and Baronti, P.: A Method for Transonic Wind Tunnel Corrections. AIAA J., vol. 11, no. 1, Jan. 1973, pp. 63-66.

5. Sears, W. R.: Self-Correcting Wind Tunnels. Calspan Report No. RK-5070-A-2, July 1973; also Aeronaut. J., vol. 78, Feb.-Mar. 1974, pp. 80-89.

6. Goodyer, M. J.: A Low Speed Self Streamlining Wind Tunnel. AGARD-CP-174, Fluid Dynamics Panel Symposium on Wind Tunnel Design and Testing Techniques, London, England, Oct. 1975, pp. 13-1-13-8.

7. Chevallier, Jean-Pierre: Soufflerie Transsonique a Parois Auto-Adaptables. AGARD-CP-174, Conference Proceedings on Wind Tunnel Design and Testing Techniques, Oct. 1974, pp. 12-1-12-8.

8. Ganzer, Uwe: Windkanäle mit adaptiven Wänden zur Beseitigung von Wandinterferenzen. Zeitschrift fur Flugwissenchaften und Weltraumforschung, vol. 3, no. 2, 1979, pp. 129-133; also NASA TM-75501, 1979.

9. Goodyer, M. J.; and Wolf, S. W. D.: The Development of a Self-Streamlining Flexible Walled Transonic Test Section. AIAA Paper 80-0440, Mar. 1980.

10. Ganzer, U.: Adaptable Wind Tunnel Walls for 2-D and 3-D Model Tests. ICAS Paper 23-3, 12th Congress of the International Council of Aeronautical Sciences, Munich, Germany, Oct. 1980.

11. Archambaud, J. P.; and Chevallier, J. P.: Utilization de Parois Adaptables pour les Essais en Courant Plan. AGARD-CP-335, Conference Proceedings on Wall Interference in Wind Tunnels, London, England, May 1982, pp. 14-1-14-14.

12. Wolf, S. W. D.; Cook, I. D.; and Goodyer, M. J.: The Status of Two- and Three-Dimensional Testing in the University of Southampton Transonic Self-Streamlining Wind Tunnel. AGARD-CP-335, Conference Proceedings on Wall Interference in Wind Tunnels, London, England, May 1982, pp. 15-1-15-14.

13. Ganzer, U.: On the Use of Adaptive Walls for Transonic Wind Tunnel Testing. AGARD-CP-335, Fluid Dynamics Panel Specialists Meeting on Wall Interference in Wind Tunnels, London, England, May 1982, pp. 13-1-13-8.

14. Vidal, R. J.; Catlin, P. A.; and Chudyk, D. W.: Two-Dimensional Subsonic Experiments with an NACA 0012 Airfoil. Calspan Report No. RK-5070-A-3, Dec. 1973.

15. Vidal, R. J.; Erickson, J. C., Jr.; and Catlin, P. A.: Experiments with a Self-Correcting Wind Tunnel. AGARD-CP-174, Fluid Dynamics Panel Symposium on Wind Tunnel Design and Testing Techniques, London, England, Oct. 1975, pp. 11-1-11-13.

16. Sears, W. R.; Vidal, R. J.; Erickson, J. C., Jr.; and Ritter, A.: Interference-Free Wind Tunnel Flows by Adaptive-Wall Technology. ICAS Paper 76-02, 10th Congress of ICAS, Ottawa, Canada, Oct. 1976; also J. of Aircraft, vol. 14, no. 11, Nov. 1977, pp. 1042-1050.

17. Vidal, R. J.; and Erickson, J. C., Jr.: Experiments on Supercritical Flows in a Self-Correcting Wind Tunnel. AIAA Paper 78-888, Apr. 1978.

18. Erickson, J. C., Jr.; Wittliff, C. E.; Padova, C.; and Homicz, G. F.: Adaptive-Wall Wind-Tunnel Investigations. Calspan Report No. 6040-A-2, Feb. 1981.

19. Kraft, E. M.; and Parker, R. L., Jr.: Experiments for the Reduction of Wind Tunnel Wall Interference by Adaptive-Wall Technology. AEDC Report No. AEDC-TR-79-51, Oct. 1979.

20. Parker, R. L., Jr.; and Sickles, W. L.: Two-Dimensional Adaptive-Wall Experiments. AEDC-TR-80-63, Feb. 1981.

21. Satyanarayana, Bodapati; Schairer, Edward T.; and Davis, Sanford S.: Adaptive-Wall Wind Tunnel Development for Transonic Testing. J. of Aircraft, vol. 18, no. 4, Apr. 1981, pp. 273–279.

22. Schairer, E. T.; and Mendoza, J. P.: Adaptive-Wall Wind Tunnel Research at Ames Research Center. AGARD-CP-335, Fluid Dynamics Panel Specialists' Meeting on Wall Interference in Wind Tunnels, London, England, May 1982, pp. 16-1–16-13; also NASA TM-84237, 1982.

23. AGARD Advisory Report No. 174: Windtunnel Capability Related to Test Sections, Cryogenics and Computer-Windtunnel Interaction. The Windtunnel Testing Techniques Sub-Committee of the Fluid Dynamics Panel, Apr. 1982.

24. Parker, R. L., Jr.; and Sickles, W. L.: Application of Adaptive-Wall Techniques in a Three-Dimensional Wind Tunnel with Variable Wall Porosity. AIAA Paper 80-0157, Jan. 1980.

25. Parker, R. L., Jr.; and Erickson, J. C., Jr.: Development of a Three-Dimensional Adaptive-Wall Test Section with Perforated Walls. AGARD-CP-335, Fluid Dynamics Panel Specialists Meeting on Wall Interference in Wind Tunnels, London, England, May 1982, pp. 17-1–17-14.

26. Davis, S. S.: A Compatibility Assessment Method for Adaptive-Wall Wind Tunnels. AIAA J., vol. 19, Sept. 1981, pp. 1169–1173.

27. Sleeman, William C., Jr.; Klevatt, Paul. L.; and Linsley, Edward L.: Comparison of Transonic Characteristics of Lifting Wings from Experiments in a Small Slotted Tunnel and the Langley High-Speed 7- by 10-Foot Wind Tunnel. NACA RM-L51F14, 1951.

28. Glauert, H.: The Interference of Wind Channel Walls on the Aerodynamic Characteristics of an Aerofoil. Aeronautical Research Committee, R&M No. 867, Mar. 1923.

29. Hess, J. L.: Calculation of Potential Flow about Arbitrary Three-Dimensional Lifting Bodies. Report MDC-J5679-01, Douglas Aircraft Co., Inc., Oct. 1972.

TABLE 1.– TIME BUDGET FOR EACH CYCLE

	Time, min	% of total time
Balance data acquisition and reduction	0.5	1.7
Pressure data acquisition and reduction	1.0	3.3
LV positioning	8.0	26.8
LV data acquisition and reduction	7.0	23.3
Outer flow calculation	1.0	3.3
Pressure change calculation	1.0	3.3
Valve adjustments (manual)	11.5	38.3
Total	30.0	100.0

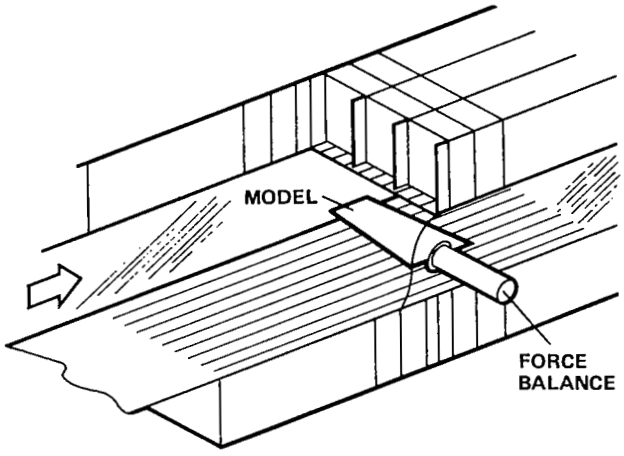

Figure 1.– Schematic of three-dimensional adaptive-wall test section.

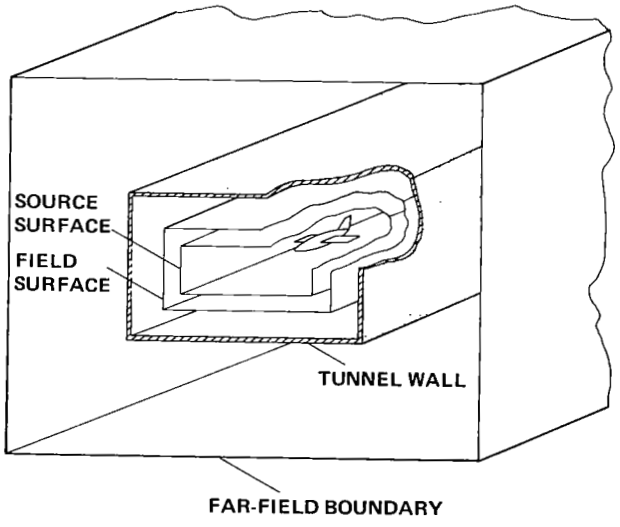

Figure 2.– Geometry for adaptive-wall algorithm.

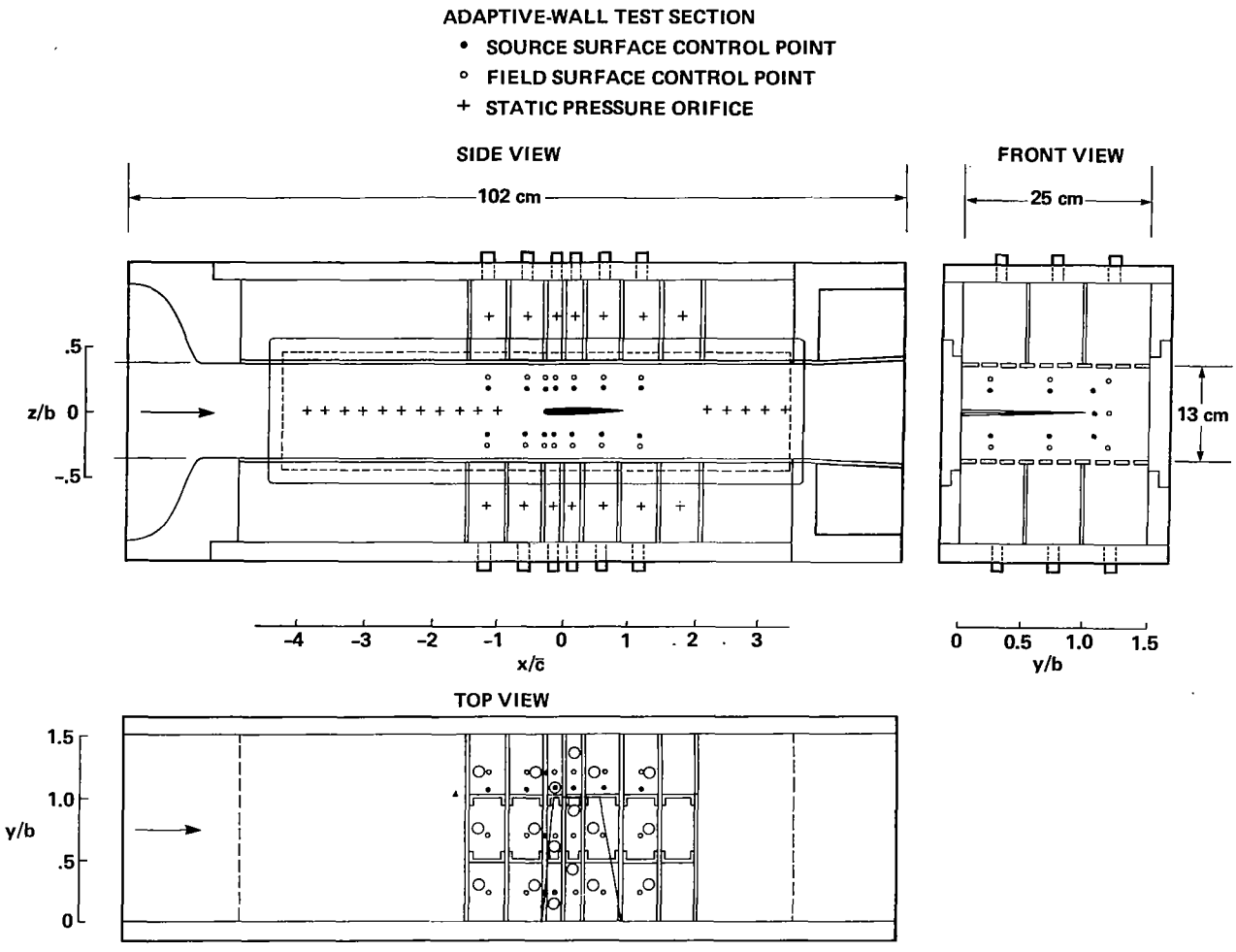

Figure 3.– Adaptive-wall test section.

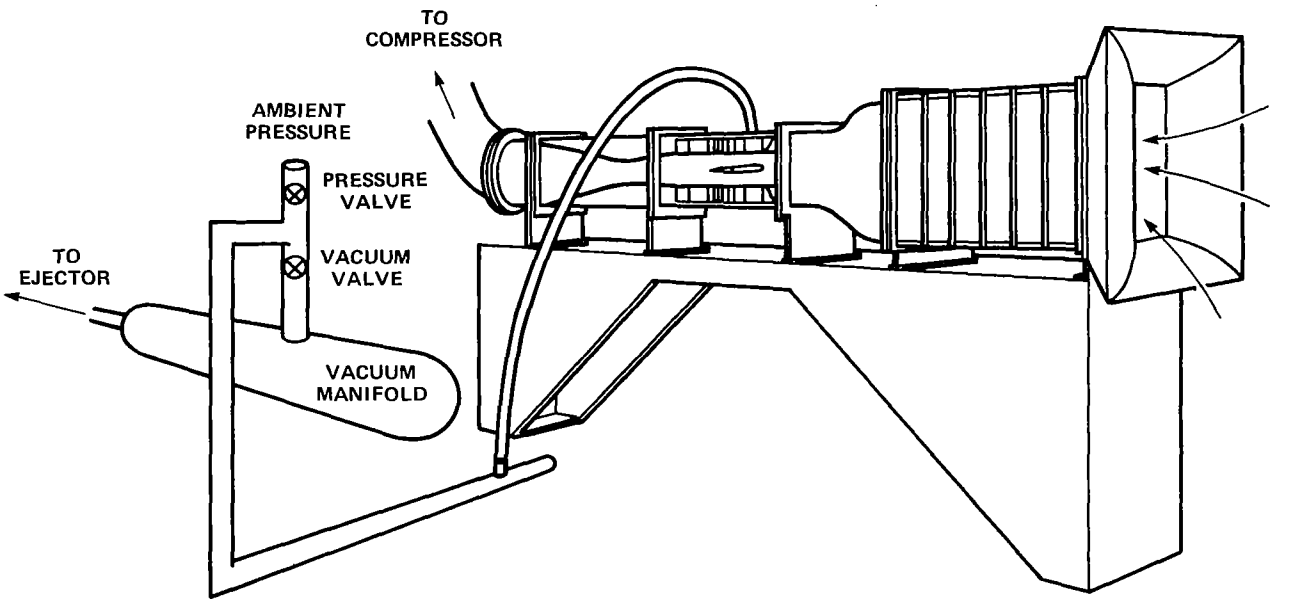

Figure 4.– 25- by 13-cm adaptive-wall wind tunnel showing how one plenum is connected to the auxiliary air system.

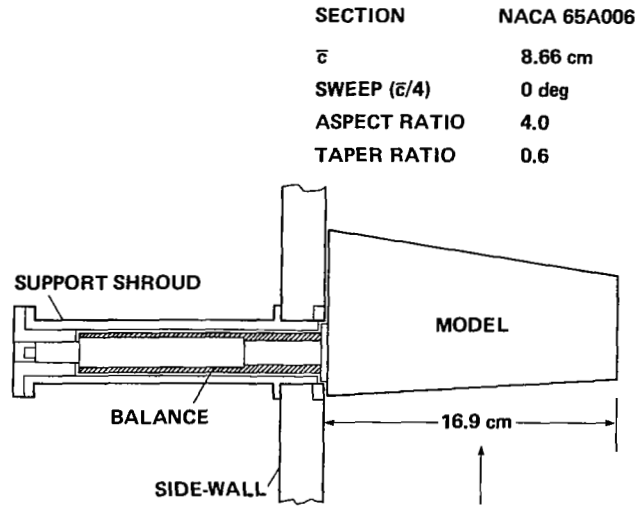

Figure 5.– Model and balance assembly.

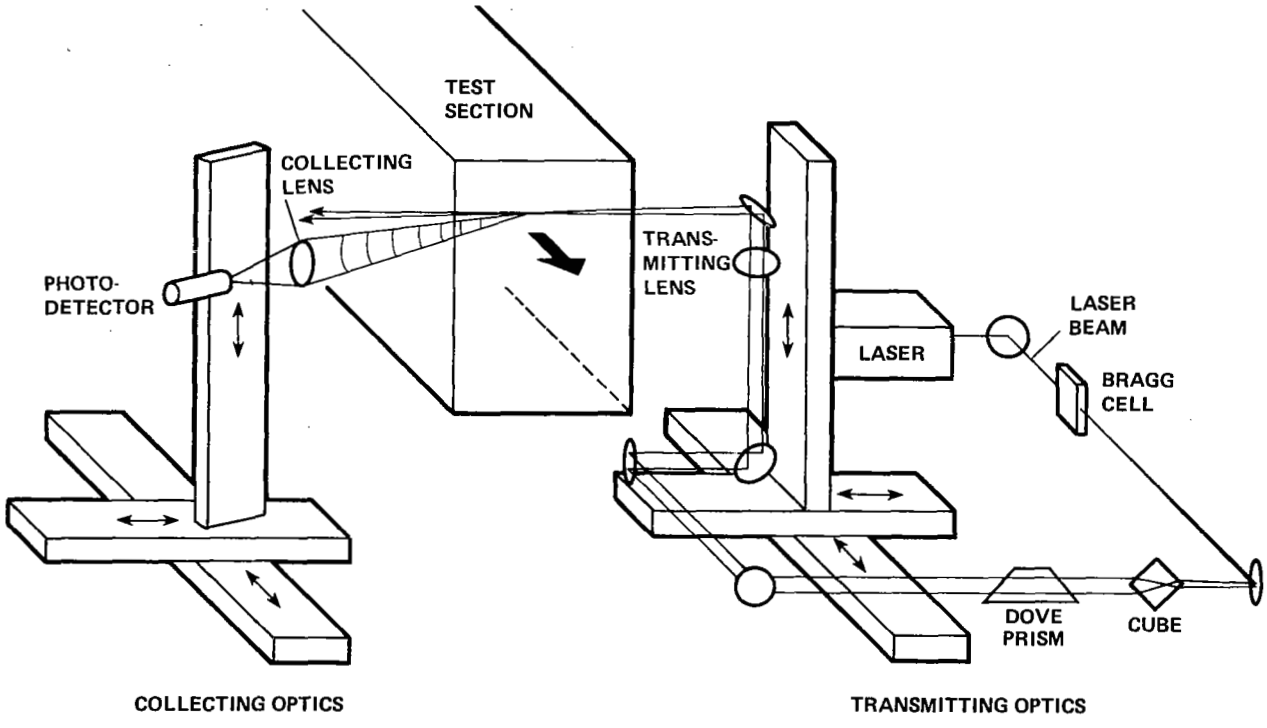

Figure 6.– Schematic of laser velocimeter.

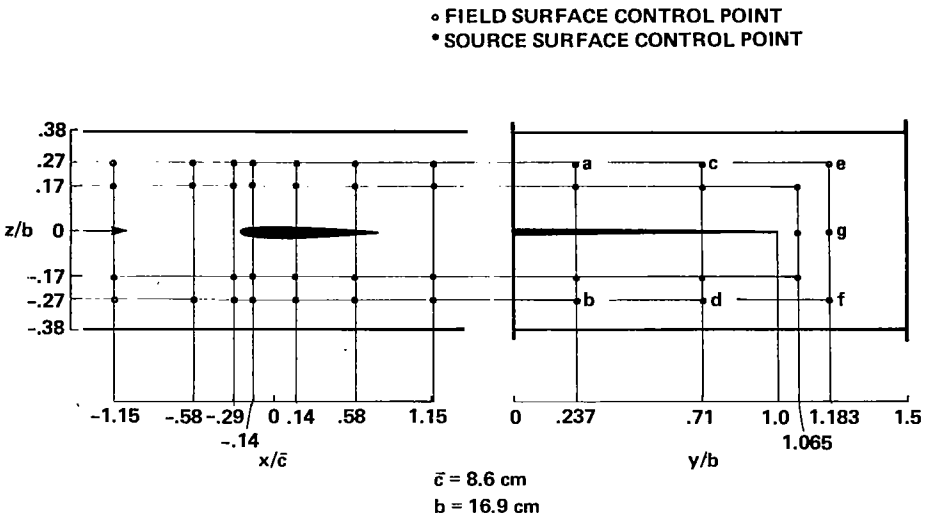

Figure 7.— Normalized coordinates of LV measurement locations.

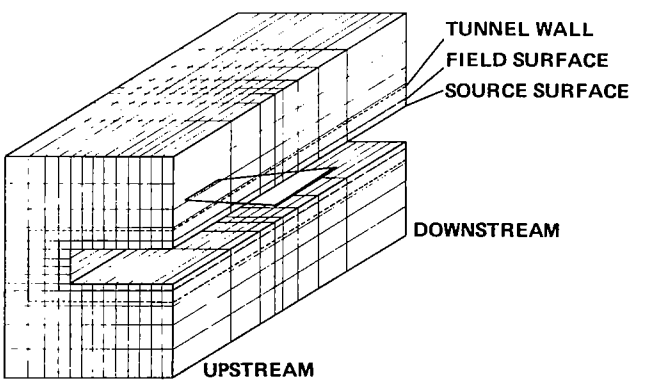

Figure 8.— Outer-flow computation space.

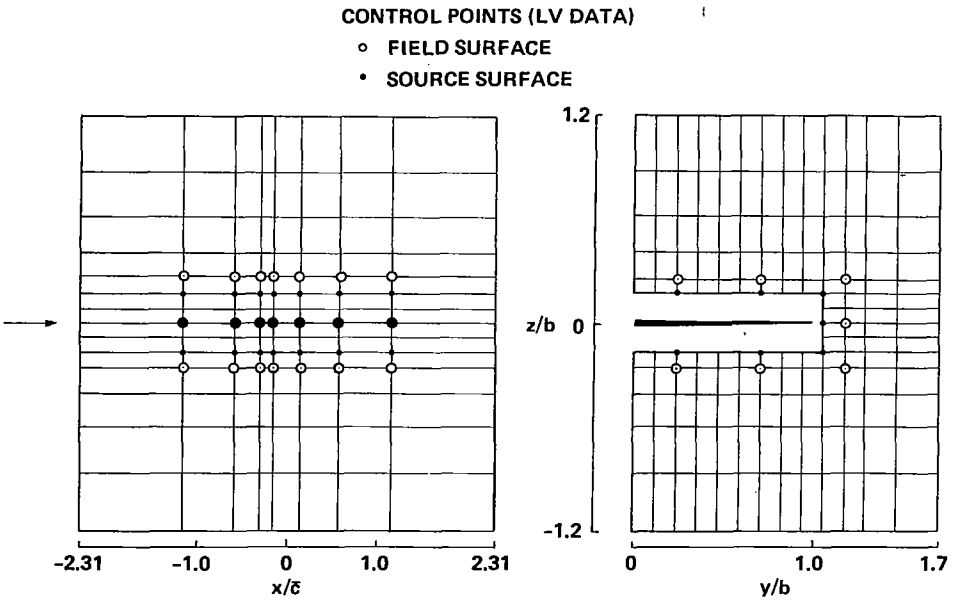

Figure 9.– Outer-flow computation mesh.

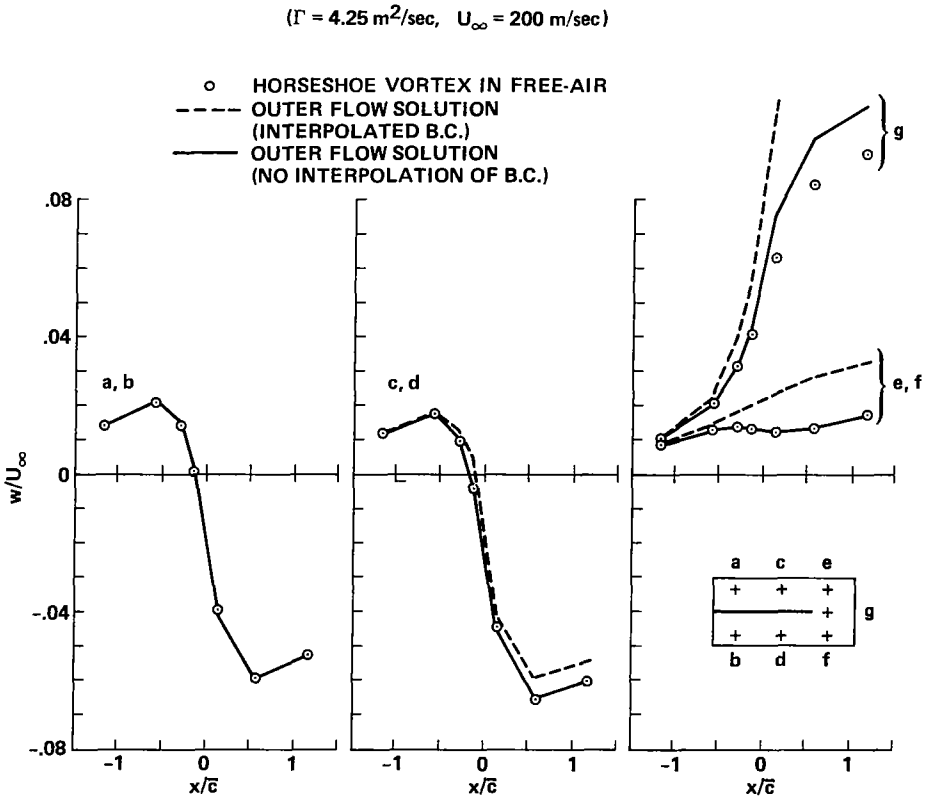

Figure 10.– Outer-flow solution check case.

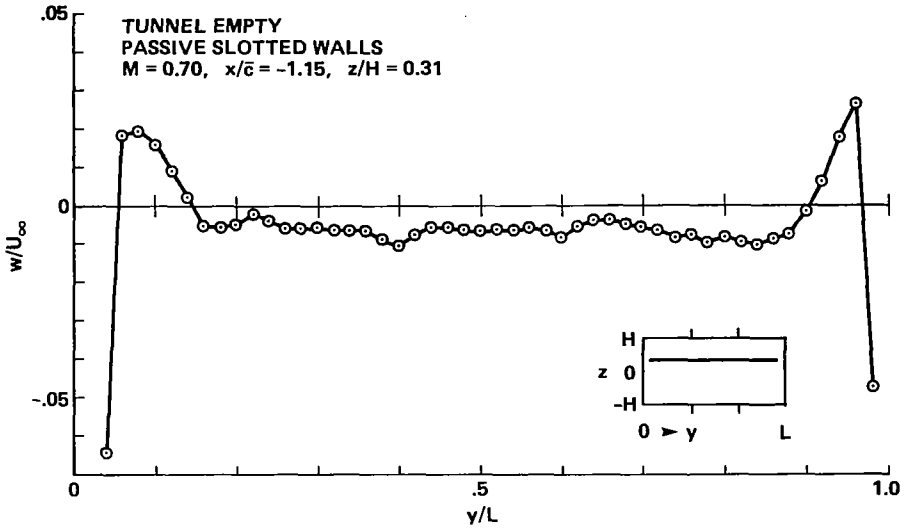

Figure 11.– Vertical velocity profile along a cross-stream line (tunnel empty, passive slotted walls).

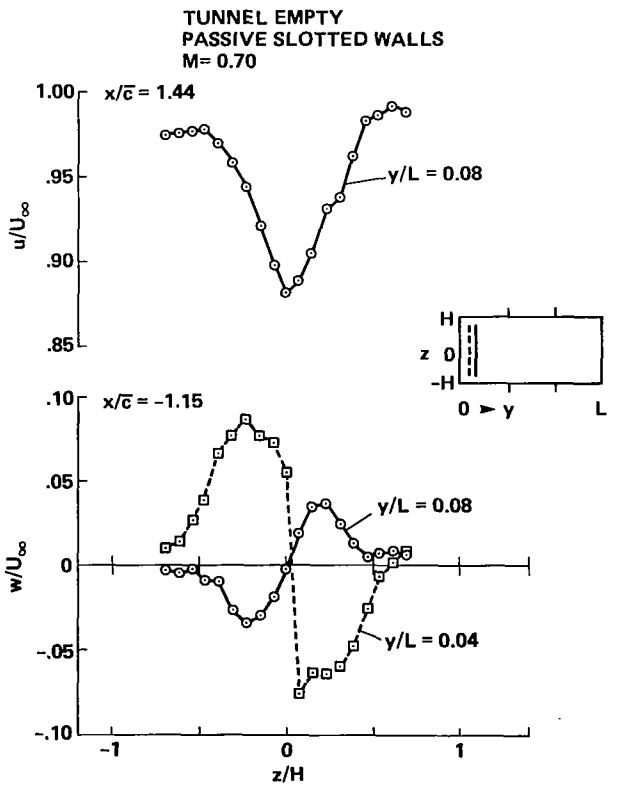

Figure 12.– Streamwise and vertical velocity distributions near one sidewall (tunnel empty, passive slotted walls).

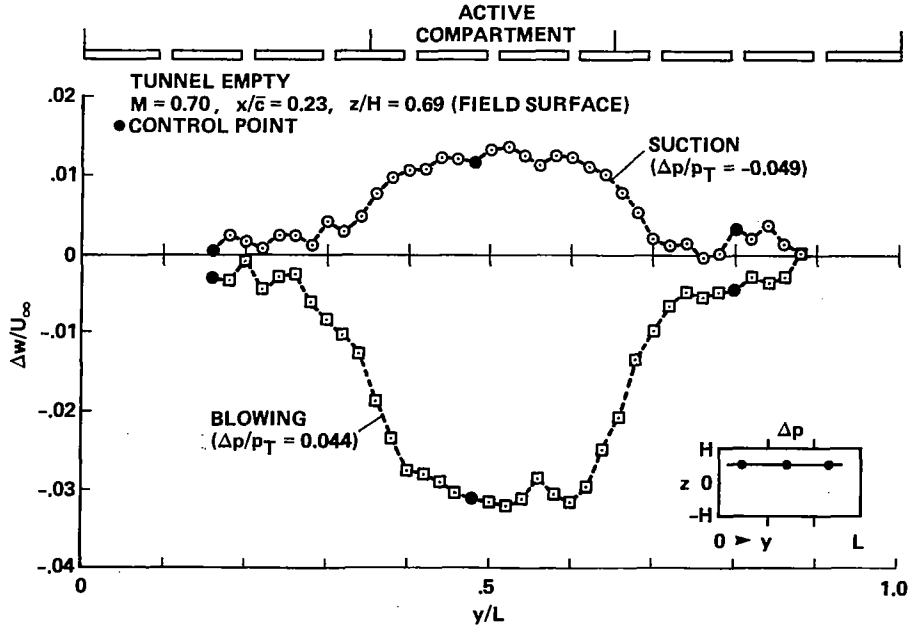

Figure 13.– Influence of pressure changes in one plenum compartment on the upwash distribution along a cross-stream line below the active compartment.

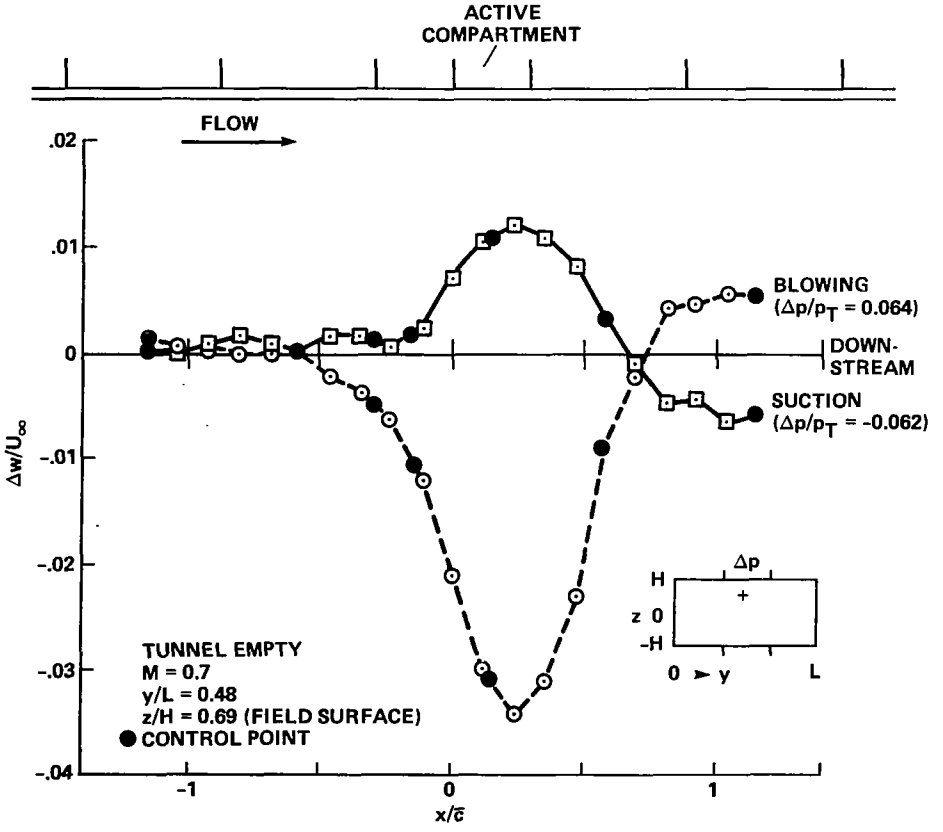

Figure 14.– Influence of pressure changes in one plenum compartment on the upwash distribution along a longitudinal line.

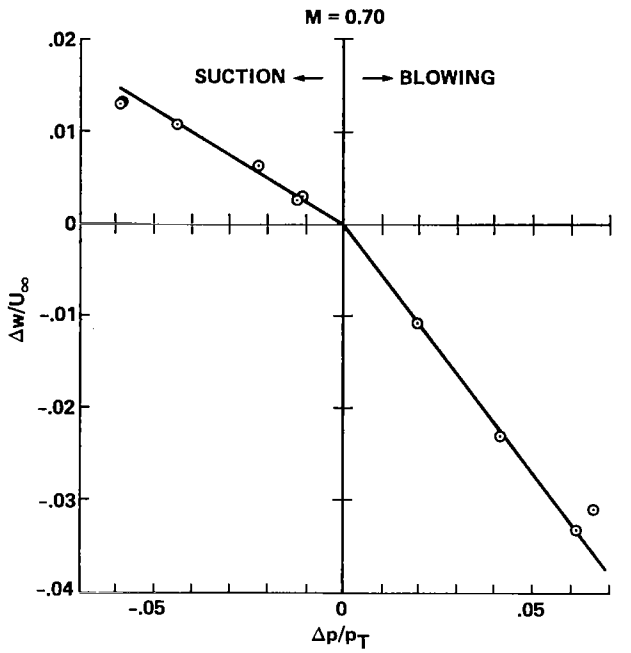

Figure 15.– Typical relationship between the pressure in one plenum compartment and the upwash at a control point on the field surface immediately below the active compartment.

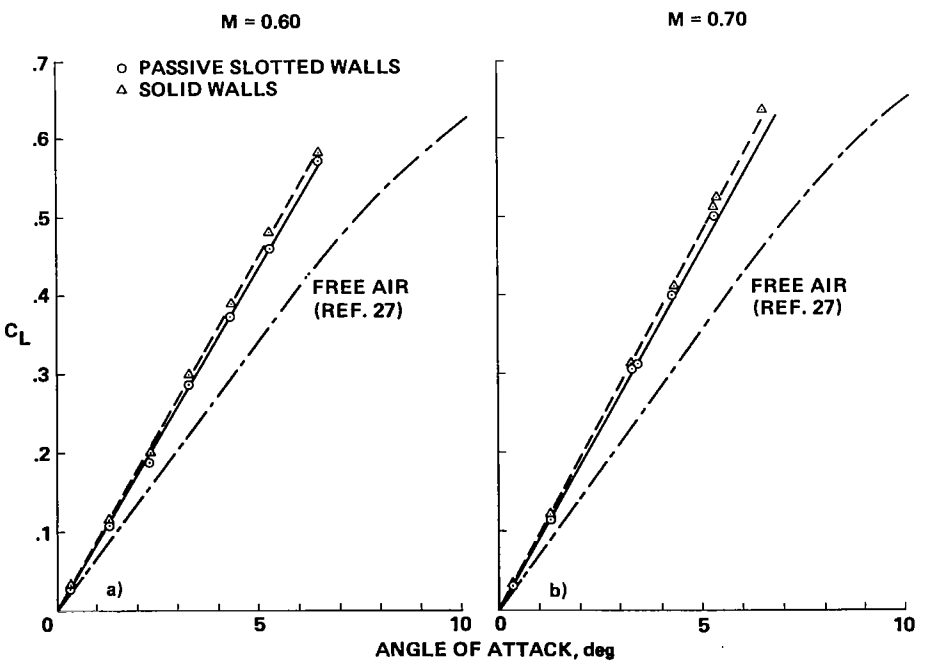

Figure 16.– Lift coefficient of the model as a function of angle of attack (passive walls).

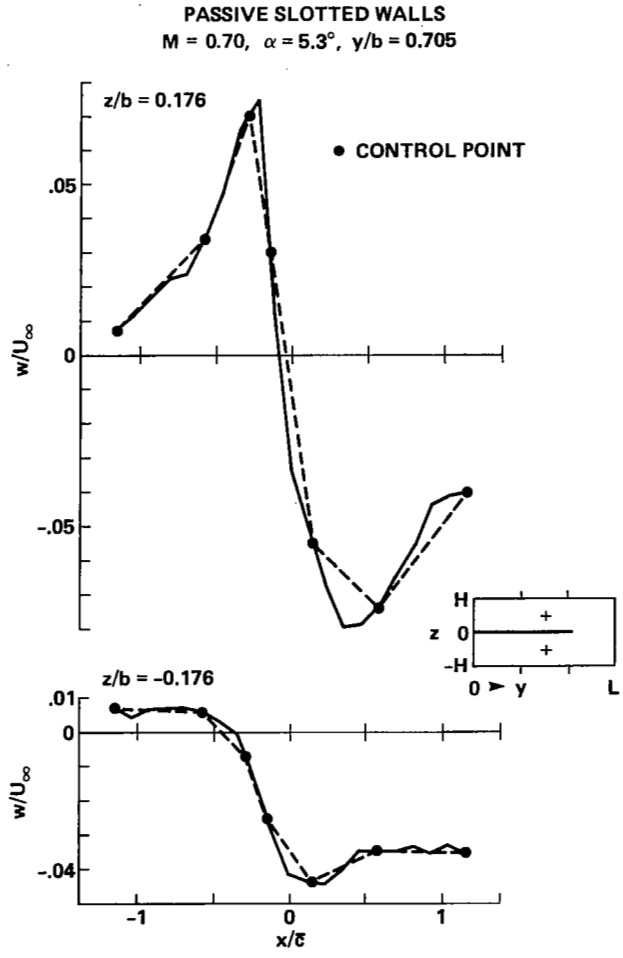

Figure 17.– Upwash distributions along axial lines on the source surface.

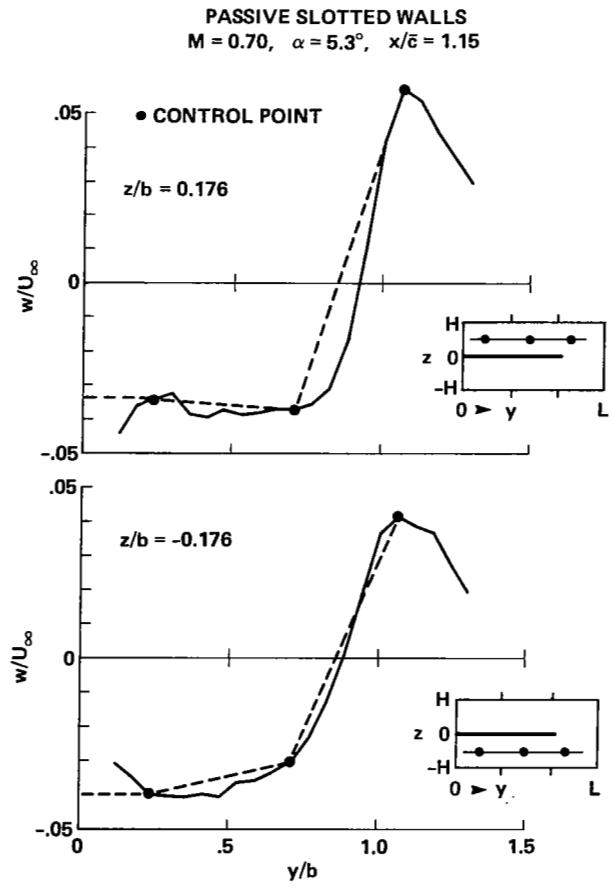

Figure 18.– Upwash distributions along spanwise lines on the source surface.

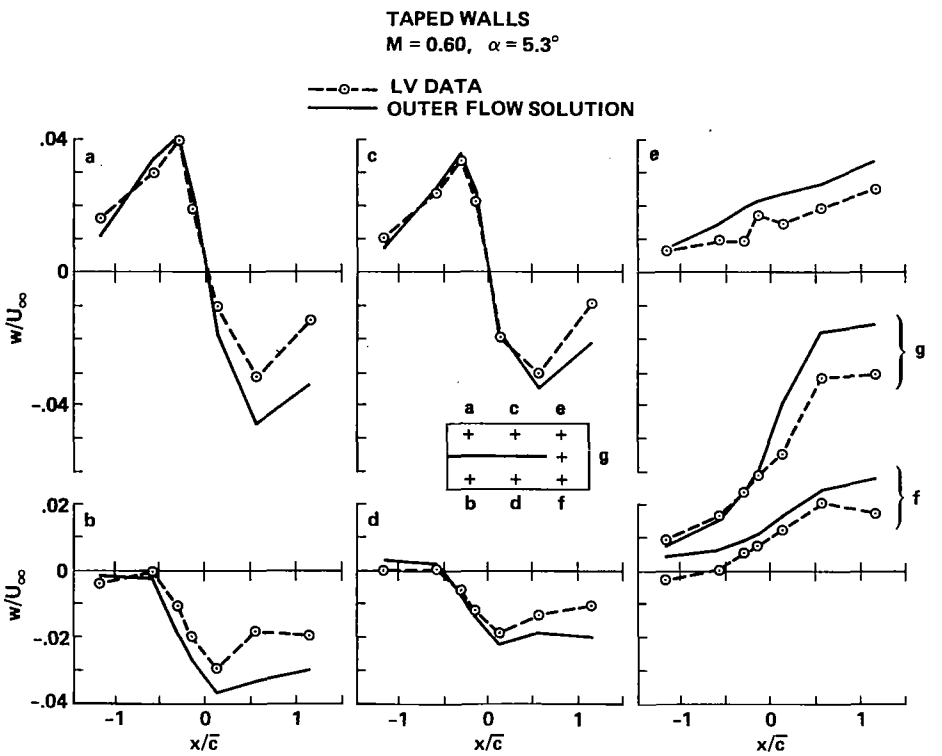

Figure 19.– Comparison of outer-flow solution and experimental upwash data at the field surface (taped walls, $M = 0.60$, $\alpha = 5.3°$).

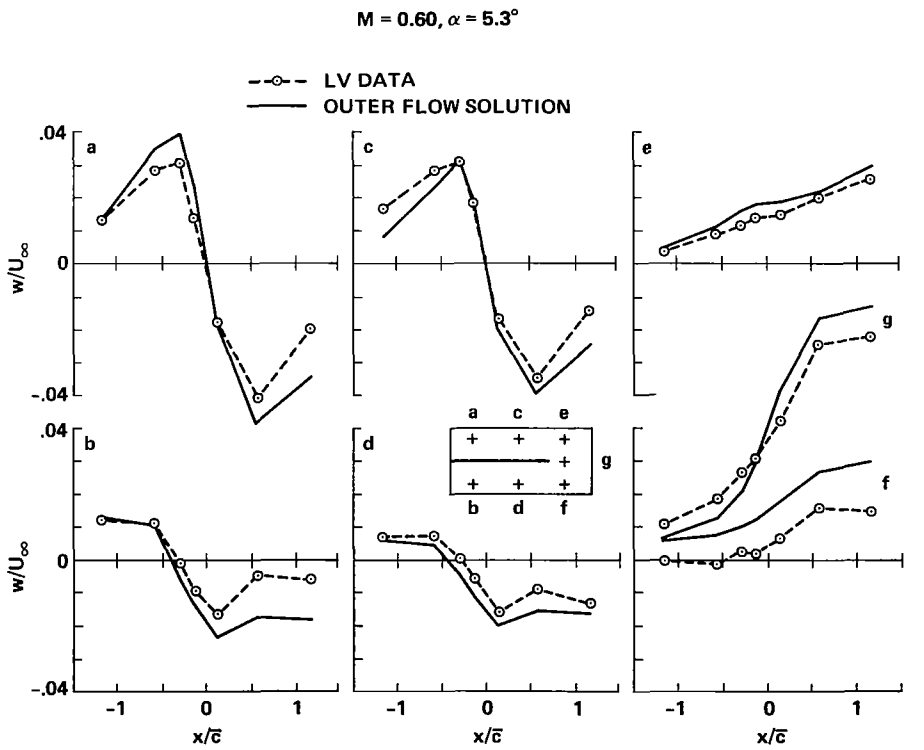

Figure 20.– Comparison of outer-flow solution and experimental upwash data at the field surface (passive slotted walls, $M = 0.60$, $\alpha = 5.3°$).

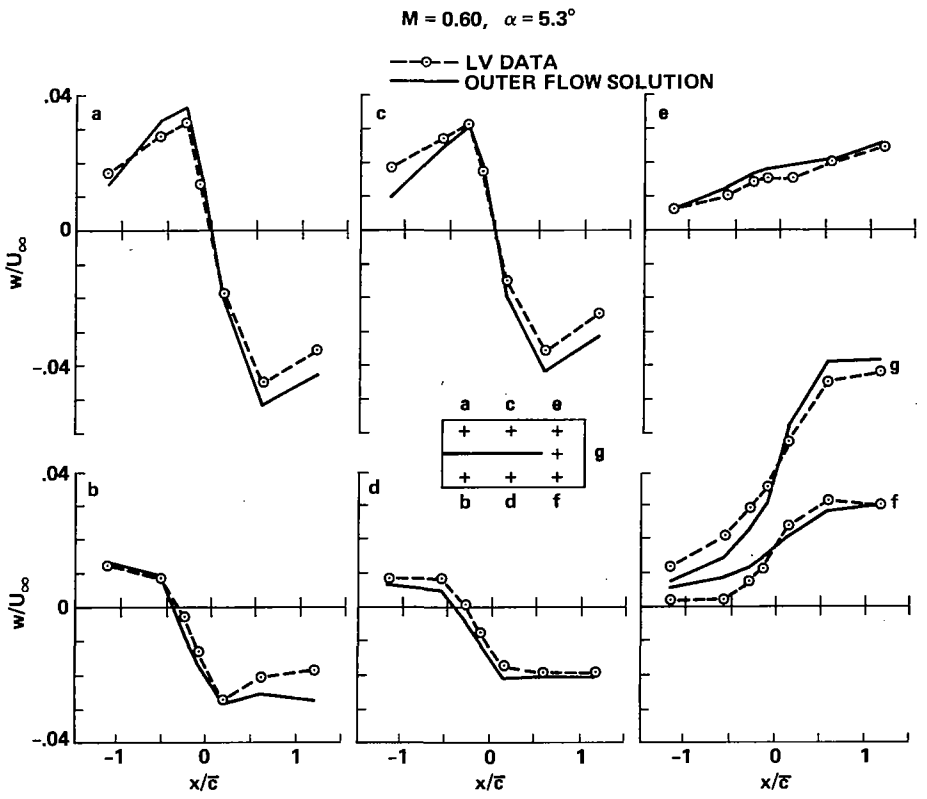

Figure 21.– Comparison of outer-flow solution and experimental upwash data at the field surface (adapted walls, $M = 0.60$, $\alpha = 5.3°$).

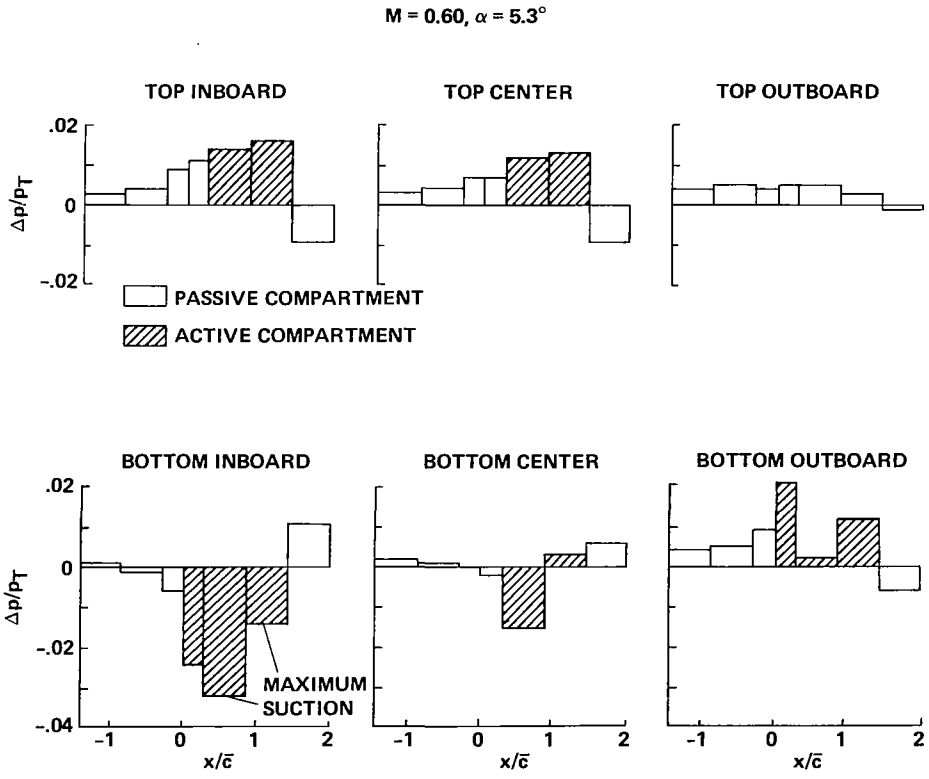

Figure 22.– Changes in plenum compartment pressures produced by the adaptive-wall procedure, $M = 0.60$, $\alpha = 5.3°$.

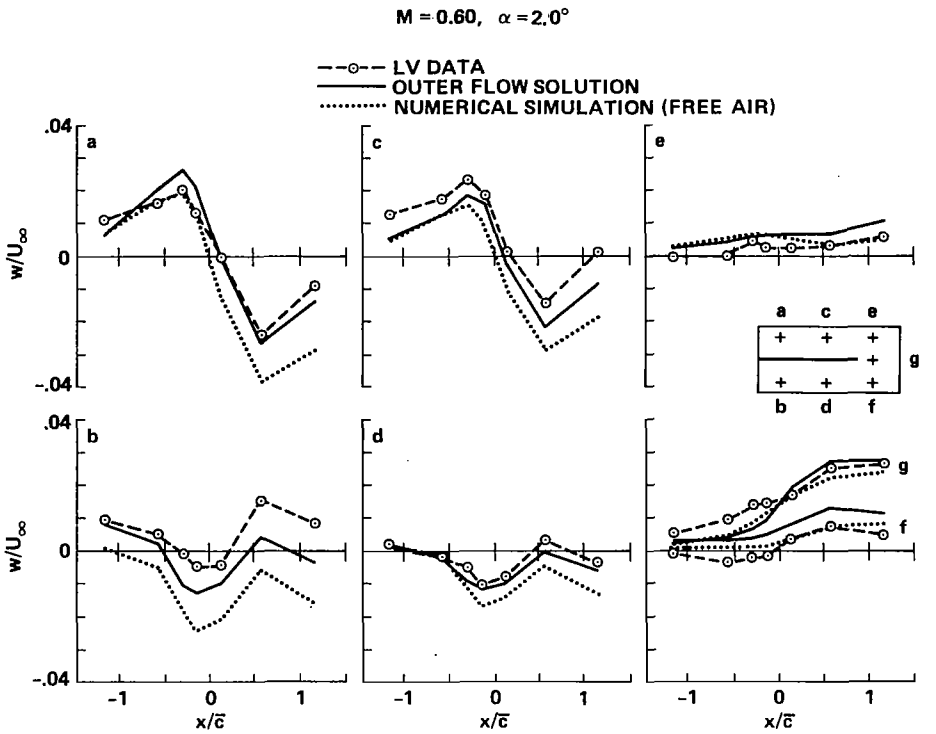

Figure 23.– Comparison of outer-flow solution, experimental data (passive slotted walls) and numerical simulation (free air, unpublished paper by J. P. Mendoza, ARC), $M = 0.60$, $\alpha = 2.0°$.

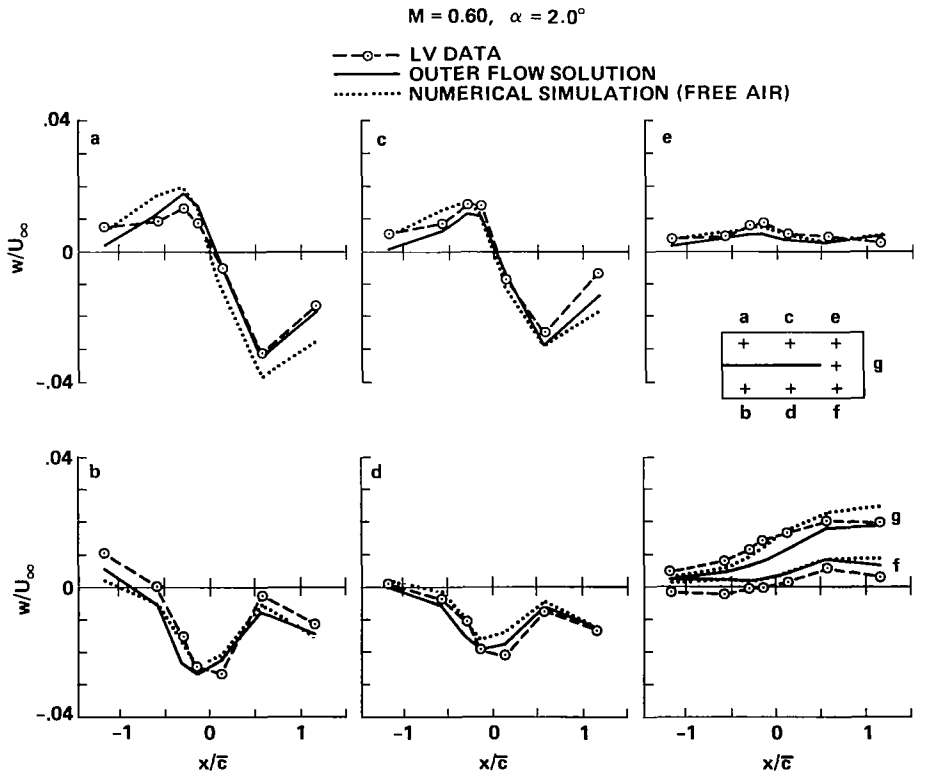

Figure 24.– Comparison of outer-flow solution, experimental data (adaptive walls), and numerical simulation (free air, unpublished paper by J. P. Mendoza, ARC), $M = 0.60$, $\alpha = 2.0°$.

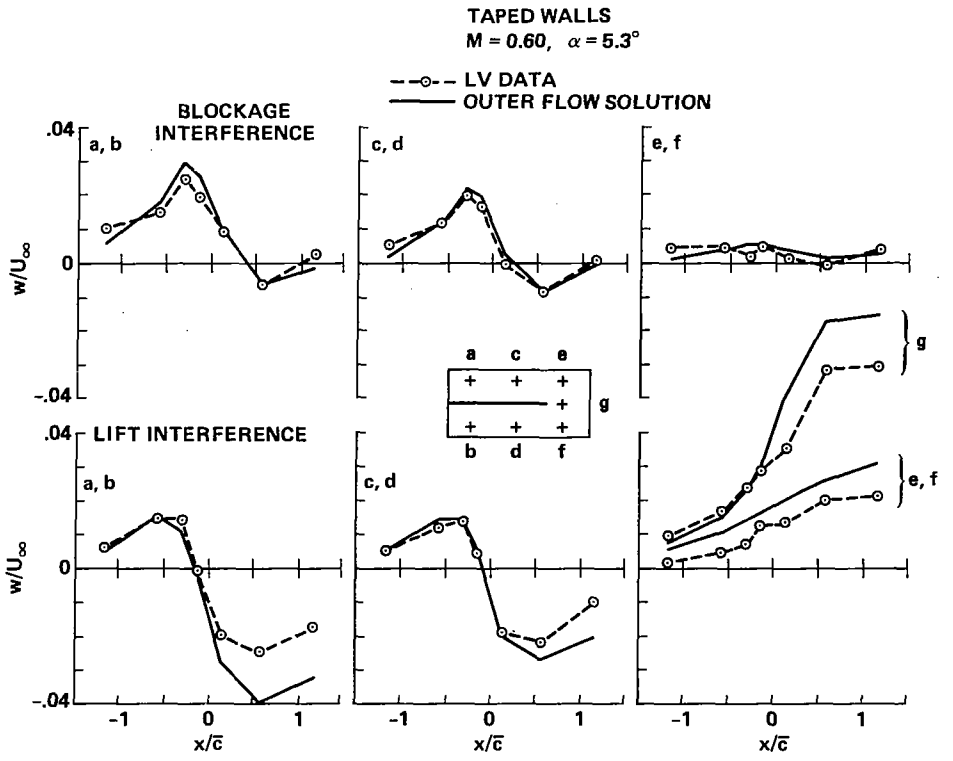

Figure 25.– Lift and blockage interference assessments (taped walls, M 0.60, $\alpha = 5.3°$).

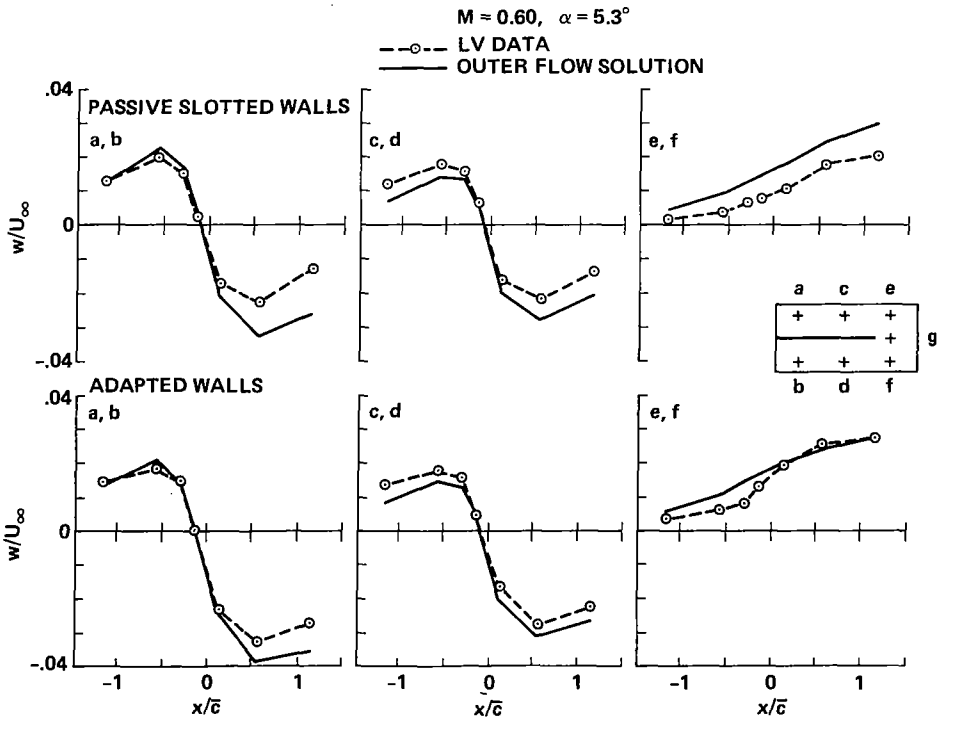

Figure 26.– Effects of wall adjustments on lift interference, $M = 0.60$, $\alpha = 5.3°$.

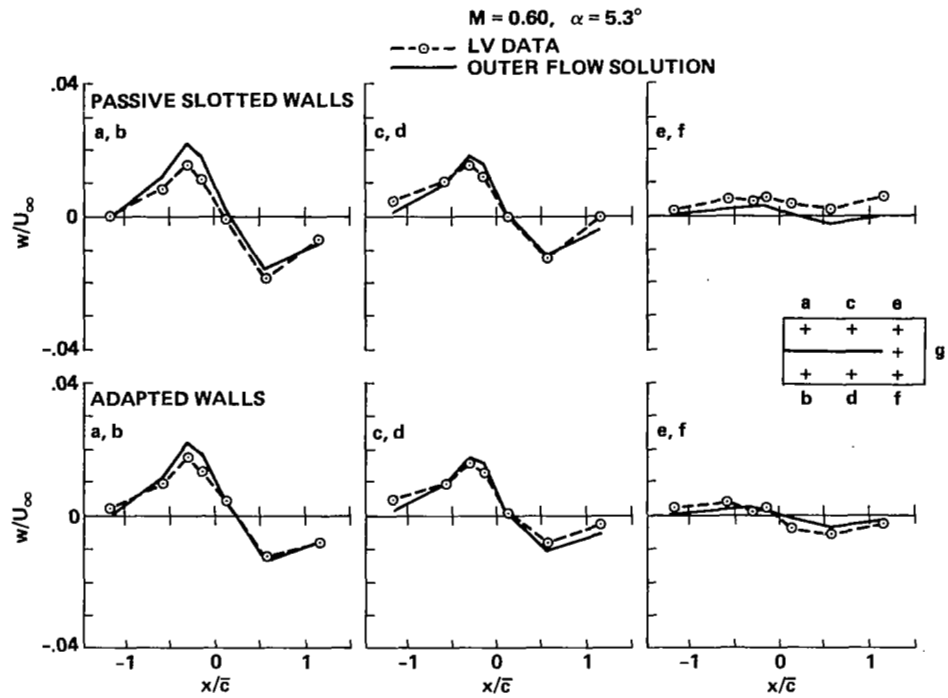

Figure 27.– Effects of wall adjustments on blockage interference, $M = 0.60$, $\alpha = 5.3°$.

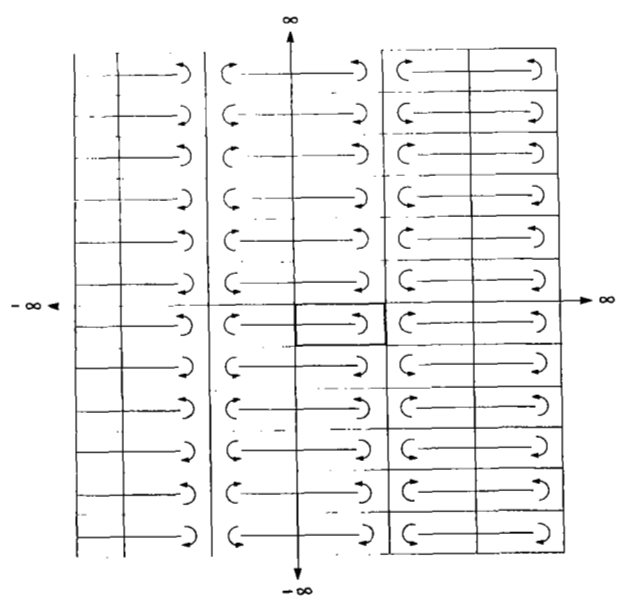

Figure 28.– Interpretation of solid-wall lift interference by the method of images.

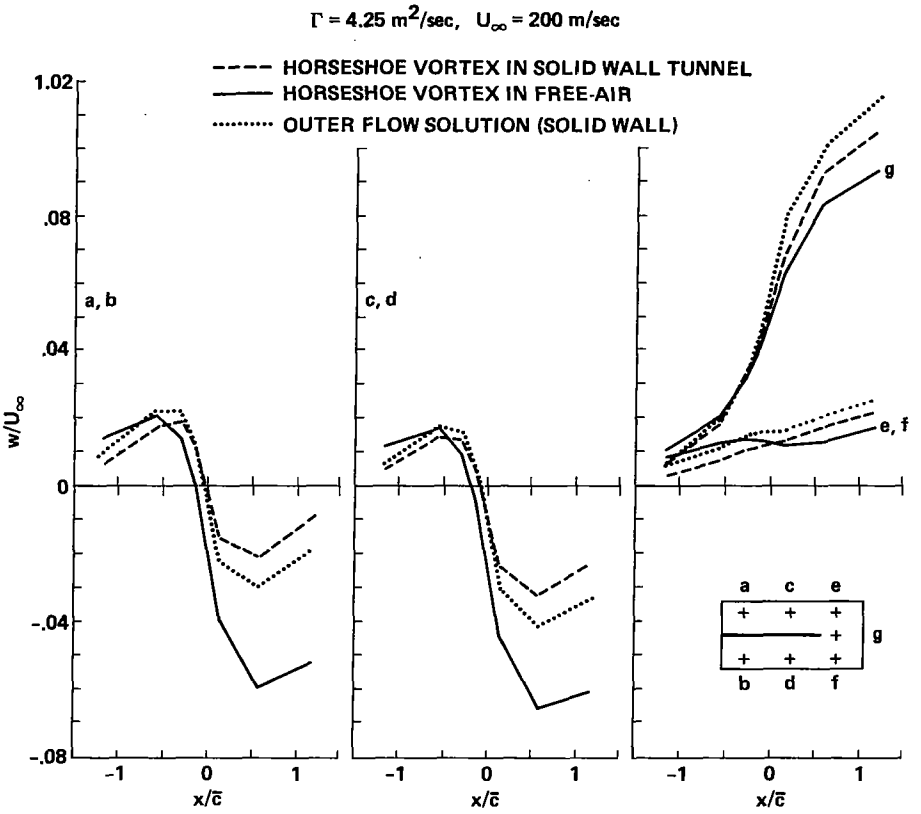

Figure 29.– Assessment of interference for a horseshoe vortex in a solid-wall wind tunnel.

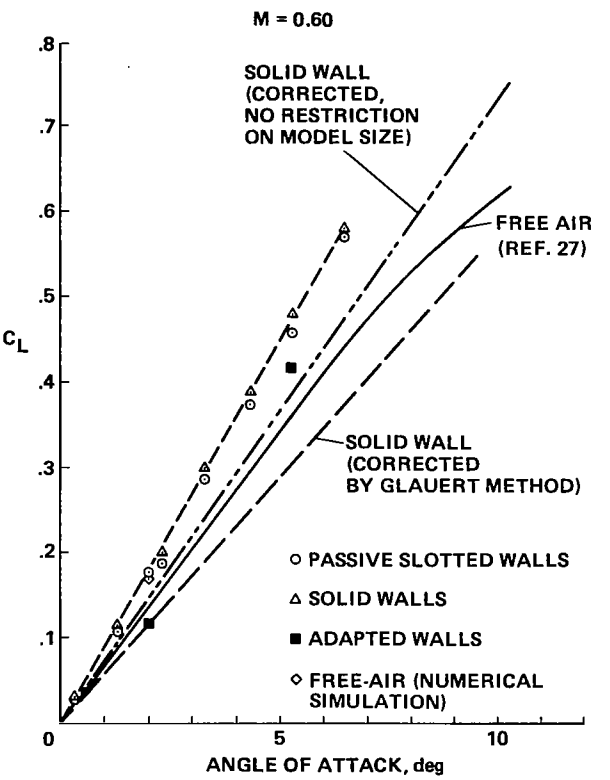

Figure 30.– Effect of wall adjustments on the model lift coefficient.

1. Report No. NASA TP -2210	2. Government Accession No.	3. Recipient's Catalog No.
4. Title and Subtitle EXPERIMENTS IN A THREE-DIMENSIONAL ADAPTIVE-WALL WIND TUNNEL		5. Report Date September 1983 6. Performing Organization Code
7. Author(s) Edward T. Schairer		8. Performing Organization Report No. A-9255 10. Work Unit No.
9. Performing Organization Name and Address NASA Ames Research Center Moffett Field, Calif. 94035		11. Contract or Grant No. 13. Type of Report and Period Covered Technical Paper
12. Sponsoring Agency Name and Address National Aeronautics and Space Administration Washington, D.C. 20546		14. Sponsoring Agency Code 505-31-51

15. Supplementary Notes

Point of Contact: Edward T. Schairer, Ames Research Center, Moffett Field, CA 94035 Ph: (415) 965-6288 or FTS 448-6288

16. Abstract

Three-dimensional adaptive-wall experiments were performed in the Ames Research Center (ARC) 25- by 13-cm indraft wind tunnel. A semispan wing model was mounted to one sidewall of a test section with solid sidewalls, and slotted top and bottom walls. The test section had separate top and bottom plenums which were divided into streamwise and cross-stream compartments. An iterative procedure was demonstrated for measuring wall interference and for adjusting the plenum compartment pressures to eliminate such interference. The experiments were conducted at a freestream Mach number of 0.60 and model angles of attack between 0 and 6°. Although in all the experiments wall interference was reduced after the plenum pressures were adjusted, interference could not be completely eliminated.

17. Key Words (Suggested by Author(s))	18. Distribution Statement		
Adaptive-wall Experiments Semispan wing model	Unclassified - Unlimited Subject Category – 02		
19. Security Classif. (of this report)	20. Security Classif. (of this page)	21. No. of Pages	22. Price*
Unclassified	Unclassified	31	A03

*For sale by the National Technical Information Service, Springfield, Virginia 22161

NASA-Langley, 1983